NUCLEAR INSTRUMENTS AND METHODS 145 (1977) 91-113 ; © NORTH-HOLLAND PUBLISHING CO.

IV. Spallation sources

PULSED SPALLATION NEUTRON SOURCES FOR SLOW NEUTRON SCATTERING*

JOHN M. CARPENTER

Argonne National Laboratory, Argonne, Illinois 60439, U.S.A.

The role of pulsed spallation neutron sources for slow neutron spectroscopy is sketched. Various methods of neutron production, and some aspects of the spallation neutron production process are outlined. Accelerators for pulsed spallation neutron sources are discussed. Materials and coolants for neutron-producing targets and moderators are surveyed. The performance of moderators and the effects of varying size, composition, and temperature are summarized. Expressions for estimating moderator performance are given. The effect of moderator-reflectors, which enhance the slow neutron beam current at low energies, are examined. The ZING-P prototype pulsed neutron source and the proposed Intense Pulsed Neutron Source are described.

Pulsed spallation sources are a new generation of sources for slow neutron spectroscopy which offer an order of magnitude improvement over currently available thermal neutron flux and several orders of magnitude greater epithermal flux.

1. Introduction

The special properties of neutrons have long been exploited for the study of condensed matter. Neutron diffraction and inelastic scattering have now become keen tools for determination of atomic and magnetic structures and excitations[1]). The range of phenomena in which neutron scattering techniques are used spans biology, chemistry, solid state physics, metallurgy, ceramics, liquids, polymers, ... providing in many cases information unobtainable by any other means. In other cases invaluable information complementary to that obtained by more traditional methods is obtained. Table 1 summarizes the unique properties of slow neutrons which have led to their wide and vigorous use.

TABLE 1

Advantages and disadvantages of neutron scattering techniques.

1. Scattering length varies irregularly among elements and isotopes (for nuclear scattering).
2. No form factor is associated with nuclear scattering.
3. Neutrons carry no charge, penetrate volume of sample.
4. Neutrons carry a magnetic moment and are a unique probe of magnetism.
5. Sources provide neutrons whose wavelength and energy are well matched to interatomic spacings and excitations in condensed matter.
6. Technique is intensity limited and costly.

Table 1 also notes a disadvantage of neutron scattering methods; that in most applications the technique is intensity limited. This is in spite of the fact that sources providing thermal neutron fluxes exceeding 10^{15} n/cm^2·s are available. For example, the highest, 1.2×10^{15} n/cm^2·s is provided by the high flux reactor at the Institut Laue Langevin, Grenoble, France. This reactor is also the most extensively instrumented neutron source which exists and supports a steadily growing program which amounted to 535 experiments in 1975. Energetic programs also exist at many other centers.

Steady state fission reactors are the most common neutron sources. However as can be observed in fig. 1[2]), reactor developments are reaching the limits of practically attainable flux. The limits are imposed by a combination of engineering limitations related to the power density in the core and by economic constraints.

Pulsed neutron sources are able to provide momentarily higher neutron fluxes than those provided by steady state reactors. Since pulsed sources operate only part time, the momentary power density, and therefore the momentary neutron flux, can be very high, while the average power density is still within practical limits. If the repetition frequency is large enough and the pulse width short enough then for a large class of neutron scattering applications the performance of

* Based on work performed under the auspices of the U.S. Energy Research and Development Administration.

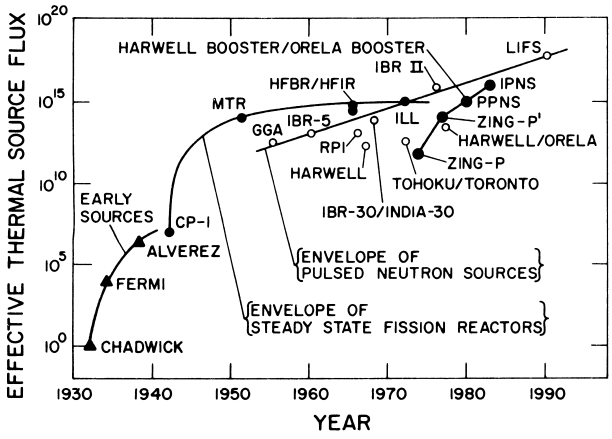

Fig. 1. Available neutron fluxes have increased with development of accelerator sources and nuclear reactors[2]). Pulsed sources are a new generation of neutron sources which will increase available fluxes by at least a factor of ten.

pulsed sources can be compared with that of steady sources on the basis of pulsed source peak flux versus steady source average flux. Time-of-flight (TOF) methods have been developed and used at steady state reactors and at a number of electron linear accelerator and pulsed reactor sources. Time-of-flight methods (using choppers) on steady sources are in general comparable in efficiency to steady state methods (for example using crystal monochromators) and are preferred for certain classes of measurements. For other applications steady state techniques are the preferred methods and there is a deep traditional commitment to steady state techniques in these areas. It is reasonable to expect that the availability in the future of major pulsed sources will lead to such developments of time-of-flight techniques that they will have a major impact in several of these areas as well. The advantages and disadvantages of pulsed sources are summarized in table 2.

TABLE 2

Pulsed neutron sources.

Advantages
1. High effective intensity is obtained for the same average neutron production.
2. Source pulse defines one element of the resolution function.
3. Background is low; source is off most of the time.
4. Spectrum is rich in epithermal neutrons.
5. Resolution $\Delta E_0/E_0$ is nearly constant.
Disadvantage
1. Time-of-flight techniques are obligatory.

Pulsed neutron sources based on the proton induced spallation process are capable of providing peak thermal neutron fluxes at least an order of magnitude greater than those available in steady reactors. These also provide peak epithermal neutron fluxes two or three orders of magnitude greater than are now available. Such an increase in available flux has not occurred since the early years of reactor development. The cost of such a source will be less than the cost of a new steady state research reactor. These increases come about because of the low average heat dissipation accompanying pulsed operation, because the spallation process is relatively efficient compared to fission and other processes and because accelerators can be built which provide the needed proton beam intensity, pulse length and repetition frequency.

2. Survey of methods of neutron production

It is useful to compare several possible mechanisms of neutron production. Features of several processes are shown in table 3; each has been used (except the last) for production of neutrons for certain purposes. Since power density limits at the source must be considered, the energy deposited per neutron produced is a very important parameter. The usefulness of each reaction depends not only on the tabulated features, but also on other factors, such as the energy and angular distribution of the neutrons, the range of the charged particle in charged particle reactions, the availability of ion sources and suitable accelerators, and criticality constraints (in the case of reactors). In the case of controlled thermonuclear reaction (CTR) devices, the feasibility of the scheme has to be demonstrated.

Neutron sources based on some of these processes have approached technological limits. The rotating target D, T source at Lawrence Livermore Laboratory is close to the power density limit of the D, T solid target sources and produces approximately $(2\text{–}3)\times 10^{12}$ n/s continuously. The 35 MeV deuteron stripping source proposed by Brookhaven National Laboratory is designed to push energy deposition limits very hard and is expected to produce 3×10^{15} n/s continuously. The 35 MeV deuteron stripping source proposed by Brookhaven National Laboratory is designed to push energy deposition limits very hard and is expected to produce 3×10^{15} n/s (average) using 7 MW of beam power on a flowing liquid lithium target. Electron bremsstrahlung photoneutron sources have ap-

TABLE 3
Features of some neutron producing mechanisms.

Process	Example	Yield	Energy deposition (MeV/n)
D, T solid target	400 keV deuterons on T in titanium	4×10^{-5} n/d	10,000
Deuteron stripping	35 MeV D on liquid Li	2.5×10^{-3} n/d	10,000
Electron bremsstrahlung photoneutron	100 MeV e^- on ^{238}U	5×10^{-2} n/e	2000
Fission	$^{235}U(n, f)$	1 n/fission	180
Spallation	800 MeV protons on ^{238}U	30 n/proton	55
D, T CTR	Laser or ion-beam imploded pellet	1 n/fusion	3

proached the heat transfer limits at the target; the Oak Ridge Electron Linac (ORELA) and the new Harwell Linac, are such examples with neutron production rates of about 2×10^{14} n/s (average) operating in a pulsed mode. The situation with steady state fission reactors is demonstrated by the trend towards saturation of fluxes as shown in fig. 1. The combination of technological and cost constraints limits the power of research reactors to about 100 MW (3×10^{18} n/s) and accompanying thermal neutron fluxes to about 10^{15} n/cm^2·s. Pulsed reactors or fission boosters such as the Soviet IBR-II, soon to be completed at Dubna, operate at average power up to 2 MW (6×10^{16} n/s). The instantaneous thermal neutron flux in IBR II will be 10^{16} n/cm^2·s, pulsing at 5/s, but the duration of the pulses, about 75 μs at high power, is a major disadvantage of pulsed reactors for spectroscopy with short wavelength neutrons. Fast burst test reactors and nuclear fission detonations can be operated only at low frequencies (about 1/h and 1/month, respectively) which makes them of little interest in the present context.

The spallation reaction has been demonstrated for use as a neutron source for a number of purposes including condensed matter research. The feasibility of high current pulsed accelerators, the high neutron yield and the low energy dissipation make it especially attractive as the base for the next generation of high flux neutron sources. Using 0.5 mA (average) 800 MeV protons and a ^{238}U target, and providing 150 nanosec source pulses at 60 Hz, the Intense Pulsed Neutron Source proposed by Argonne National Laboratory will produce 9×10^{16} n/s (average).

Laser-imploded pellet fusion reactions have been induced which produce up to 10^7 n/pulse; quite far from the energy breakeven (Lawson criterion) condition. The pulse frequency is about once per hour. The questions of the limits on pulsed laser beam intensity and the feasibility of igniting compressed pellets remain to be solved in the case of laser-imploded pellet fusion sources. There is current interest in pellet fusion using pulsed high energy ion beams. High output reactions remain to be achieved by any method but this is an interesting prospect for future high intensity neutron sources.

Table 4 compares some existing and proposed pulsed neutron sources.

3. Spallation neutron production

This section presents the most important features of the spallation neutron production mechanism. Fig. 2 shows the neutron yields for various proton energies, materials and target sizes measured by Fraser et al.[3]) – the yield is the total number of neutrons escaping from the target. A reasonable fit to the data for 10.2 cm × 60 cm long targets is the function

$$Y(E)=\begin{cases}0.1(A+20)\,(E_{\mathrm{GeV}}-0.120), & (1a)\\ (A>9,\ \text{except}\ ^{238}U)\\ \\ 50\,(E_{\mathrm{GeV}}-0.120), & (1b)\\ (^{238}U)\end{cases}\qquad (0.2\lesssim E\lesssim 1.5\ \ \mathrm{GeV}),$$

where A is the mass number of the target nuclei. For 800 MeV protons on U, the yield is estimated to be 33 n/p.

The spallation process is a multiple collision process. The first interactions of energetic protons are with nucleons loosely bound by comparison with the proton energy. The particles in the nucleon–meson cascade which follows the initial interaction go on to collide again with other particles in the same and other nuclei, until their energy is spent. Energetic neutrons (as well as protons and other particles) emerge from the target in a distribution which extends in energy up to the

TABLE 4

Some pulsed neutron sources for slow neutron scattering.

Facility	Characteristics	Average fast neutron production rate (n/s)	Source pulse width (μs)	Pulse repetition frequency (Hz)	Status
		A. Spallation sources			
ZING-P (Argonne, US)	200 MeV protons, Pb target	5×10^{11}	0.2	10	Operated 1974, 1975
ZING-P′ (Argonne, US)	500 MeV protons, W target	2.4×10^{14}	0.2	30	To be operational Spring, 1977
IPNS (Argonne, US)	800 MeV protons, U target	9×10^{16}	0.25	60	Proposed
SNS (Rutherford, UK)	800 MeV protons, U target	4×10^{16}	0.25	53	Proposed
LAMPF-WNR Los Alamos, US)	800 MeV protons W target	$(1–2) \times 10^{15}$	5–10	120	To be operational Spring, 1977
with storage ring		1×10^{15}	0.2	5–120	Proposed
KENS (Tsukuba, Japan)	500 MeV protons, ^{238}U target	3×10^{14}	0.07	15	To be operational, 1979
		B. Photoneutron sources			
ORELA (Oak Ridge, US)	140 MeV e^- Ta target	1.1×10^{14}	0.1	Up to 1000	Operating
Harwell Linac I (UK)	45 MeV e^- U target	$2. \times 10^{13}$	1.7	192	Shutdown, 1976
Harwell Linac II (UK)	60 MeV e^- U target	$2. \times 10^{14}$	2–5	150–600	To be operational Fall, 1978
Kurchatov Linac (USSR)	32 MeV e^- U target	2.2×10^{12}	0.6	Up to 120	Operating
Toronto (Canada)	27 MeV e^- W target		2.0	Up to 960	Operating
Tohoku (Japan)	250 MeV e^- W target	1.4×10^{13}	3.0	110	Operating
		C. Pulsed reactors and fission boosters, aug. power, MW			
IBR-30 (Dubna, USSR) as reactor	^{238}U	0.03	50.	5	Operating
as booster	44 MeV e^- 14 kW	0.03	1.8	100	
IBR-II (Dubna, USSR) as reactor	^{239}Pu	2 MW	75.	5–50	To be operating, 1977
as booster	30 MeV e^- 200 kW	2 MW	5.	50	

energy of the incident protons and which is strongly peaked in the forward direction. After the cascade, nuclei left in a state of excitation cool off by evaporating neutrons (and some other particles). In heavy nuclei, fissions may be induced with consequent further production of neutrons evaporated by fission products.

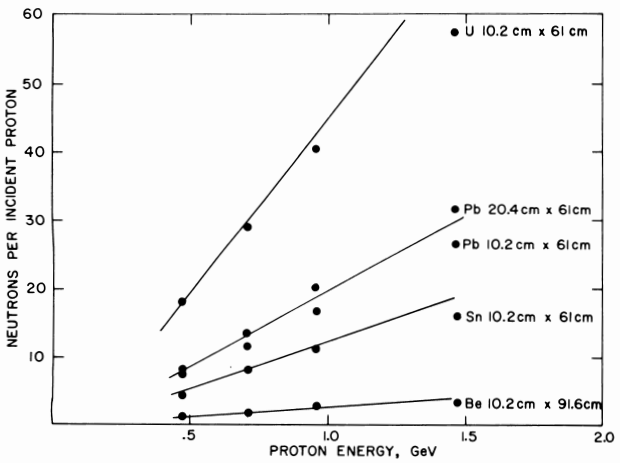

Fig. 2. Measured neutron yield vs proton energy for various targets[3]).

The evaporation component of the spectrum is nearly isotropic with a characteristic temperature of a few MeV. Virgin neutrons may make several collisions in the target before emerging, softening the spectrum somewhat. In this complex process few photons are produced. The main contribution to photon production in spallation targets accompanies the induced fissions; in non-fissioning targets, photon production is very small.

The spectrum of neutrons emerging from various targets has been calculated by Fullwood et al.[4]) using Monte Carlo codes following the description of the spallation process outlined above. Neutron yields depend on target size and are somewhat smaller for smaller targets.

Fig. 3. shows spectra for 15 cm diameter $\times$ 30 cm long targets of lead and uranium. The spectra consist of two components, the cascade

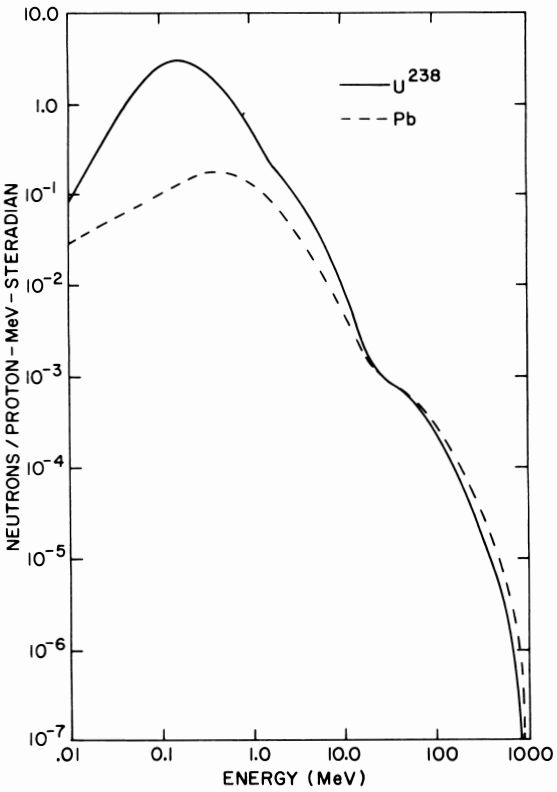

Fig. 3. Comparison of 4π neutron spectra for ^{238}U and Pb cylinders 15 cm diam., 30 cm long with 800 MeV protons incident on axis[4]).

component extending up to the proton energy 800 MeV, and the evaporation component which is dominant up to about 20 MeV. In the spectrum for the uranium target of fig. 3, the evaporation component contains about 97% of the neutrons, for the lead target, about 95%. Even though the cascade neutrons are a small fraction of the total, these dominate shielding requirements, and necessitate thicker shields than are usual in reactors.

Neutrons are not produced uniformly in the target, but are spread out over a distance comparable with the range of protons in target materials. A reasonably accurate empirical relationship for the range R is

$$\rho R(E_p) = 233\, Z^{0.23}\,(E_{GeV} - 0.032)^{1.4}\,,$$

$$Z \gtrsim 10, \quad 0.1 \lesssim E \lesssim 1 \text{ GeV}. \qquad (2)$$

For 800 MeV protons in uranium ($\rho = 18.7$ g/cm^3) the range is 25 cm. Fullwood et al.[4]) have also computed the axial distribution of neutrons produced, fig. 4. Shown in the figure is a line representing the exponential decrease of the neutron production density in the mid range of the target. The relaxation length is identifiable with the mean free path of high energy nucleons. At the incident end is a "buildup" effect, and at distance near the proton range the production density decreases toward zero.

The mean free path for collisions of high energy ($E \gtrsim 50$ MeV) nucleons can be estimated from Ashmore's formula[5]) for the total inelastic cross section

$$\sigma_{inel} = 15.9\pi A^{\frac{2}{3}} \text{ mb/nucleus}. \qquad (3)$$

For uranium ($\rho = 18.7$ g/cm^3) the mean free path thus computed is 11 cm.

The energy of the proton beam is left *in the target* in part as nuclear separation energy, and in part as sensible heat. Spallation protons, neutrons, etc. contribute to the sensible heat by ionizations and collisions as do the fragments and particles of fission while significant energy leaves the target as kinetic energy of the neutrons and other particles, to be deposited elsewhere. The question of the energy deposited per neutron produced is thus fairly

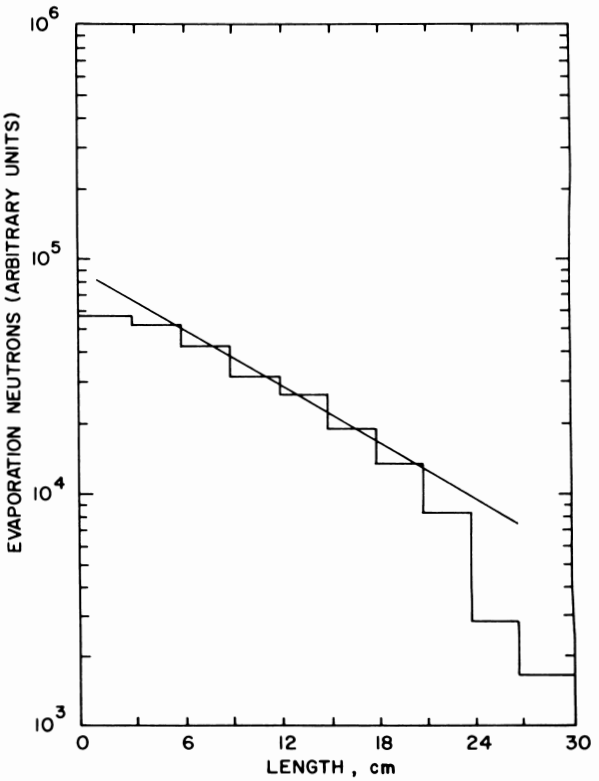

Fig. 4. Radial and axial distribution of the production of evaporation neutrons in a 7.5 cm radius, 30 cm long ^{238}U target with 800 MeV protons incident on axis[4]).

complex and dependent on target size as well as material and proton energy and is especially influenced by the presence of fissions. Fig. 5 shows the neutron yields and heat per neutron calculated by Fraser et al.[3]) for 10 cm diameter × 60 cm long Pb and ^{238}U targets. The heat per neutron decreases with increasing proton energy and levels off. For 800 MeV protons on Pb the calculations of Fraser give 30 MeV/neutron (480 MeV/proton) and on U, 55 MeV/n (1650 MeV/proton). The difference in heat generation and neutron production between Pb and U can be accounted for satisfactorily as being due to fissions in U. The difference between the heat produced per 800 MeV proton for Pb and for U is 1170 MeV/proton. Since each fission deposits about 180 MeV locally, this extra heat represents about 6.5 fissions/proton. Assuming that the difference between the prediction of eq. (1a) and the actual yield for U represents the fission contribution, one finds 17.5 n/p produced due to fission. The net neutron yield per fission, 2.7 n/fission is very reasonable.

Delayed neutrons are produced in targets in which fissions take place. In ^{238}U the delayed neutron yield is approximately 0.05 neutrons/fission[6]). These contribute a time-independent background source which may be troublesome in some measurements. These are not multiplied as in pulsed reactors and fission boosters. The total delayed neutron yield is around 1% of all neutrons produced by a ^{238}U spallation source.

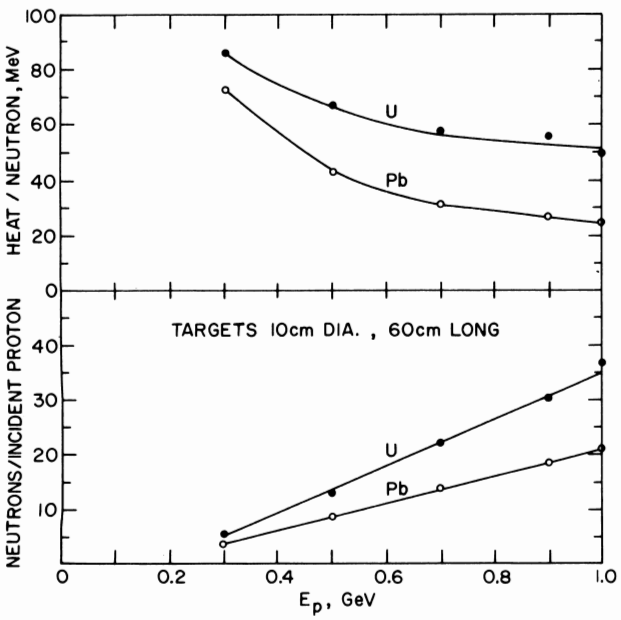

Fig. 5. Heat production per neutron produced and neutron yield vs incident proton energy[3]).

Neutrons can also be produced between pulses due to fissions in ^{235}U or ^{239}Pu which are induced by slow neutrons returning to the target from surrounding moderators. Therefore depleted ($\lesssim 0.02\%$ ^{235}U) uranium rather than natural uranium is desirable and ^{239}Pu, which is produced by neutron capture in small ^{238}U targets at the rate of about 3 atoms/proton, must not be allowed to accumulate. ^{235}U and ^{233}U are also produced by spallation, but at smaller rates. The return neutron fission effect can be reduced by decoupling the target from its surroundings by a layer of boron.

4. Accelerators for pulsed spallation neutron sources

For use in the broadest range of neutron scattering research the primary neutron pulse should be less than the time width of the moderated pulse at the highest energies of interest, a few tenths μs. For neutron spectroscopy with energies in the millivolt range, the time between pulses should be tens of ms. The proton energy should be high enough to produce high neutron yields, that is greater than a few hundred MeV. Protons with energies greater than about 1 GeV produce proportionately more neutrons, but these are spread out over source lengths which exceed the slowing down length in moderator materials and give roughly constant neutron fluxes albeit in a greater volume. Since accelerator capital and operating costs increase linearly with energy and shielding against the greater numbers and higher energies of neutrons becomes costly, proton energies much above 1 GeV are not much to be desired.

Protons rather than deuterons or heavier projectiles are best. The formula for the inelastic cross section

$$\sigma_{\text{incl}} = 38.15\pi A^{\frac{2}{3}}, \text{ (d, } ^3\text{He, } ^4\text{He)} \qquad (4)$$

implies only 2.4 times greater spallation yield per particle than for protons [eq. (3)] although then only when the energy per nucleon is comparable with the proton energy. The added cost and difficulty of accelerating heavier particles probably implies higher cost than proton acceleration for the same performance[7]). The questions of neutron production in targets bombarded with these heavier particles remain to be examined in detail.

These conclusions may be altered in consequence of such analysis.

Linear accelerators are an apparently attractive choice to produce the required high proton currents. These operate most efficiently with duty cycle factors of a few %, implying pulses either too long or too frequent for slow neutron spectroscopy. For example, the 800 MeV LAMPF linear accelerator produces 500 μs long macropulses at 120 Hz; the pulses are too long to be of direct use. 5 μs long pulses will be diverted from the LAMPF 500 μs pulse to a target for neutron production in the Weapons Neutron Facility. Cyclotrons such as TRIUMF[8]) are essentially steady state devices although they can be pulsed with the maximum current equal to the steady state current.

Synchrotrons have traditionally been low average current machines but recent developments[7]) of rapid cycling synchrotrons have made possible their use as high current accelerators. Pulse lengths are inherently short; single turn extraction implies a pulse length (due to bunching) less than $2\pi R_{ave}/\beta c$, where R_{ave} is the machine average radius. For 800 MeV protons and $R_{ave} = 20$ m this is 500 ns. The cycling frequency can be as high as 60 Hz as in the proposed Argonne High Intensity Synchrotron. High accelerated charges are made possible by stripping injection of negative hydrogen ions[9]).

Proton storage rings are very similar to synchrotrons, the main difference being the constant magnetic field and rf frequency. The construction of both a high energy linac or a cyclotron and a storage ring is more costly than construction of a synchrotron with low energy linac injector although addition of a proton storage ring to an existing accelerator as is proposed at Los Alamos is somewhat less costly than construction of a synchrotron.

Thus proton synchrotrons or storage rings for ~ 1 GeV protons, employing H^- injection are the apparent best choices for use in a neutron source for slow neutron spectroscopy.

5. Materials and coolants for spallation neutron targets

Spallation neutron targets for slow neutron spectroscopy should be of high-mass-number material in order to provide highest neutron yields, and as compact as possible so as to couple efficiently to moderators. The conflicting requirements of high average density and adequate cooling are to be compromised in any design. Material of high density, having high thermal conductivity and tolerant of high operating temperatures leads to compact targets with minimal dilution due to coolant. Destructive phase transitions must be avoided. Materials must exhibit minimal growth and other degradation due to thermal cycling, irradiation damage or accumulation of fission and spallation products or of hydrogen from the stopped proton

TABLE 5

Some properties of materials for high power spallation neutron targets.

Material	Density (g/cm^3)	C (J/g·°C)	T_{melt} (°C)	(W/cm·°C)	Neutron yield for 800 MeV protons (n/p)	A
Ta	16.6	0.14	2 996	0.54	13.7	181
W	19.3	0.13	3 410	1.8	13.9	184
Pb	11.4	0.12	328	0.35	15.4	207
Bi	9.7	0.12	271	0.084	15.6	209
U	18.7	0.12	1 133	0.25	35.	238
U-5 w/o Fs [a]	18.0	0.12	999	0.11	29.	—
U-Springfield's adjusted alloy[b]	18.7	0.12		0.11	35.	—
U-10 w/o Mo	16.3	0.13	1 410	0.19	29.	—
Pb-56 w/o Bi	10.3	0.63	125	0.10	15.6	—
Au 3 w/o Si			363		15	
U-11 w/o Fe	~16.4		725		29	

[a] Fs = "Fissium" is a combination of elements which typically are present in reprocessed reactor fuel, and is purposefully alloyed in EBR II fuel (Argonne's Experimental Breeder Reactor II and which contribute advantageous properties to the alloy. The 5% Fs consists of 2.5 w/o Mo, 0.1 w/o Zr, 1.5 w/o Ru, 0.5 w/o Pa, 0.3 w/o Rh.

[b] Springfield's cavitation adjusted alloy contains 3000 ppm Al, Fe, Ni.

beam. Void swelling is likely to be the limiting factor in high power uranium targets. The properties of a few materials of high mass number which have been considered for targets are in table 5.

Tantalum and tungsten are attractive because of their high density, high thermal conductivity and melting temperature. Solid lead was used in early measurements because of its ready availability, but otherwise has little to recommend it as has solid bismuth. Uranium and its alloys are especially attractive because of the high neutron yield combined with high density, but their low thermal conductivities are disadvantageous. Much is known about their properties, metallurgy and irradiation behavior from extensive study in connection with nuclear reactor fuel development. Uranium in alpha phase exhibits a destructive alpha beta phase transition at 660°C. U-5 w/o Fs (see table 5, footnote a) and Springfield's Adjusted Alloy have been thoroughly studied particularly as regards thermal cycling and radiation growth. For example the fractional volume change upon 1% burnup of U-5 w/o Fs in this alloy at 600 °C is 3%. γ-phase stabilized U-10 w/o Mo has been much used as fast burst reactor fuel, but is subject to phase transformation after only brief time at 500 °C. Flowing Pb–Bi eutectic was chosen as the target material in the 40 MW target proposed for the Canadian ING project[3]), and is being used in the 400 kW target of the TRIUMF Thermal Neutron Facility[8]).

Solid target material must be appropriately subdivided in order that internal temperatures be kept within tolerable ranges. At some very high power densities conventional solid targets become unfeasible for this reason, and pebble-bed, slurry or flowing liquid targets would be required. The properties of U–Fe and Au–Si eutectics are listed in table 2 as an indication of possibilities for high yield, very high power targets.

Coolants must of course be compatible with target and cladding materials. The appropriate coolant depends on the power density in the target, the object being to cool the target adequately to avoid excessive internal temperatures. Representative values of performance parameters of various coolants evaluated under not-too-extreme conditions are given in table 6.

He gas cooling is suitable for low power density targets consisting of high thermal conductivity material and is attractive because of the low induced radioactivity. Water cooling is very attractive because of the relatively high heat transfer coefficients, but to avoid flow instability in applications with parallel flow channels, either the heat flux must not exceed that for which local boiling sets in, or the channels must be orificed. Boiling water makes possible very high heat fluxes but orificing (therefore high pressure drops) must be provided, and in any case is limited by the requirement to avoid burnout at the critical heat flux. Liquid metals enable very high heat fluxes in systems with only very modest pressures and pressure drops; boiling problems appear only at such high surface heat fluxes that it is the internal temperature variation in solid targets which limits performance.

6. Moderators for pulsed spallation neutron sources

Neutrons are slowed down from source energies of about 1 MeV to energies of interest for slow neutron spectroscopy ($\lesssim 10$ eV) by moderators placed close by the neutron source (proton target). These must provide the shortest possible pulses of highest possible intensity. The arrangement of

TABLE 6

Performance of various coolants for spallation neutron targets.

Coolant	Film coefficient h (W/cm^2·°C)	Local boiling heat flux q_{LB} (W/cm^2)	Critical heat flux q_{crit} (W/cm^2)
Gas (e.g., He)	0.1	–	–
Water			
(single phase)	1.–3.	200	–
(boiling)	7.–15.	–	300
Liquid metal (e.g., NaK)	10.–30.		2000

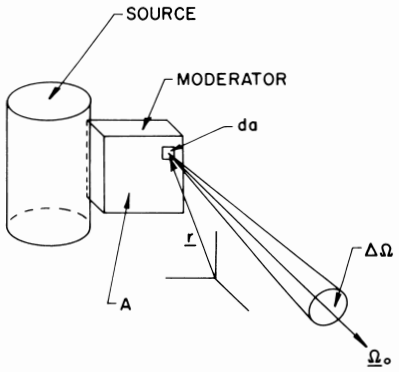

Fig. 6. Schematic arrangement of source and moderator.

source and moderator is shown schematically in fig. 6.

The intensity of neutrons from a moderator can be conveniently described in terms of the instantaneous "beam current" response function per source neutron $I(E, \boldsymbol{\Omega}_0, t)$, which is the number of neutrons emitted from the viewed moderator surface, per unit time around time t after a δ-function source pulse, per unit energy around energy E, per unit solid angle around direction $\boldsymbol{\Omega}_0$, per neutron generated by the source. $I(E, \boldsymbol{\Omega}_0, t)$ is related to $n(\boldsymbol{r}, E, \boldsymbol{\Omega}_0, t)$ the neutron density at $\boldsymbol{r}$ on the moderator surface, per unit energy, per unit solid angle, at time t after a source pulse, per neutron generated by the source, as in eq. (5),

$$I(E, \boldsymbol{\Omega}_0, t) = \int_A \mathrm{d}a v\, n(\boldsymbol{r}, E, \boldsymbol{\Omega}_0, t). \tag{5}$$

For a source which produces $S_N(t')$ neutrons per unit time at time t', the observed instantaneous beam current $i(E, \boldsymbol{\Omega}_0, t)$ is

$$i(E, \boldsymbol{\Omega}_0, t) = \int \mathrm{d}t'\, S_N(t')\, I(E, \boldsymbol{\Omega}_0, t - t'). \tag{6}$$

The time average beam current is

$$\begin{aligned} i(E, \boldsymbol{\Omega}_0) &= \left[\frac{1}{T}\int_0^T \mathrm{d}t'\, S(t')\right]\left[\int_0^{\infty} \mathrm{d}t\, I(E, \boldsymbol{\Omega}_0, t)\right] \\ &= \bar{S}_N\, \bar{I}(E, \boldsymbol{\Omega}_0), \end{aligned} \tag{7}$$

where $\bar{S}_N$ is the time average number of neutrons generated by the source, and $\bar{I}$ is the total intensity in a pulse.

The time average flux at a point a distance L in direction $\boldsymbol{\Omega}_0$ from the moderator is related to $\bar{i}(E, \boldsymbol{\Omega}_0)$ in a simple way

$$\bar{\phi}(E, L) = \frac{i(E\boldsymbol{\Omega}_0)}{L^2} = \frac{\bar{S}_N\, \bar{I}(E, \boldsymbol{\Omega}_0)}{L^2}, \tag{8}$$

since the solid angle subtended by $1\ \mathrm{cm}^2$ at distance L is just $1\ \mathrm{cm}^2/L^2$.

Moderator spectra and pulse widths can be varied by varying their material composition, their size, their temperature, or by adding absorbers. These techniques are all useful in narrowing the pulse widths. In general shorter pulses imply lower intensities, but the object of moderator design is to reach a compromise which optimizes the performance and cost of instruments for the intended applications. Michaudon[10]) has studied the effects of varying moderator parameters, mostly for high energy neutrons ($E \gtrsim 10$ eV) and has tabulated proton densities in a number of candidate moderator materials. (An error in his table concerning the proton density of $NH_3H_2PO_4$ results from an error in a commonly used handbook.) Michaudon's figure of merit

$$\frac{\int_{\text{pulse}} i(E, t)\, \mathrm{d}t}{\tau(E)^2}$$

is applicable to a broad class of applications.

A recent bibliography on *Condensed matter research using pulsed neutron sources,* by Mildner and Stirling[11]) contains references to the still growing literature of measurements and calculations of pulsed moderator spectra and time distributions.

6.1. The neutron pulse at high energies

The neutron density at time t following a source pulse in an infinite scattering medium, at energies large compared to the temperature and to the chemical binding energy, is[12])

$$n(E, t) = \frac{1}{2E}\,\frac{y^{2/\gamma}\, \mathrm{e}^{-y}}{\Gamma(2/\gamma)}, \tag{10}$$

which is the χ^2 distribution with $(2+4/\gamma)$ degrees of freedom. Here

$$\begin{aligned} y &= \frac{\xi}{\gamma}\Sigma_s v t, \\ \xi &= \text{mean logarithmic energy change per collision} \\ &= 1 - \alpha\varepsilon/(1-\alpha) \approx 2/A, \\ 2\xi\gamma &= \text{mean-squared logarithmic energy change per collision}, \end{aligned}$$

$$\begin{aligned} \gamma &= 1 - \frac{\frac{1}{2}\alpha\varepsilon^2}{1-\alpha-\alpha\varepsilon} \approx 4/(3A), \\ \varepsilon &= \ln 1/\alpha, \\ \alpha &= [(A-1)/(A+1)]^2, \\ \Sigma_s &= \text{macroscopic scattering cross section}, \\ A &= \text{mass number}. \end{aligned}$$

The average slowing down time and the standard deviation of the slowing down time distribution at speed v are

$$t = (1+2/\gamma)\,(\gamma/\xi\Sigma_s v), \qquad \sigma_t = \sqrt{(1+2/\gamma)}\,(\gamma/\xi\Sigma_s v). \tag{11}$$

The full width at half-maximum τ of the time distribution is proportional to the difference $\Delta y_{1/2}$ between the two solutions of the equation

$$\left[\left(\frac{y}{p}\right)\mathrm{e}^{(1-y/p)}\right] = \tfrac{1}{2}; \quad p \equiv 2/\gamma; \qquad \tau = \Delta y_{1/2}(\gamma/\xi\Sigma_s v). \tag{12}$$

TABLE 7
Neutron slowing-down properties of some materials.

Material	Σ_s (cm^{-1})	ξ	γ	$\upsilon\bar{t}$ (cm)	$\upsilon\sigma_t$ (cm)	$\upsilon\tau$ (cm)
H_2O	1.34	0.92	0.99	2.43	1.40	2.7
$(CH_2)_n$ (0.94 g/cm^3)	1.84	0.90	0.98	1.82	1.03	2.0
D_2O	0.64	0.60	0.56	6.7	3.12	6.6
Be	0.93	0.207	0.143	11.1	2.9	6.5
Graphite (1.7 g/cm^3)	0.47	0.158	0.108	28.	6.4	14.8
Fe	1.00	0.0353	0.0237	57.	6.2	14.4

Pulses from finite moderators are somewhat shorter than is indicated by the infinite medium calculations. Table 7 gives values (averaged with respect to cross sections) of these parameters for some materials.

It is clear from the table that due to their superior slowing down power $\xi\Sigma_s$, materials with largest possible hydrogen densities are most desirable for producing short pulses.

6.2. The spectrum of neutrons at high energies

At energies above 1 eV, the beam current, after a short source pulse, has approximately the same form as eq. (10)

$$i(E, \boldsymbol{\Omega}_0, t) \propto \frac{1}{2E} \frac{y^{2/\gamma} e^{-y}}{\Gamma(2/\gamma)};$$

$$y = \frac{\xi}{\gamma} \Sigma_s \upsilon t; \tag{13}$$

$$\bar{i}(E, \boldsymbol{\Omega}_0) \propto \frac{1}{\xi\Sigma_s E}, \qquad (\xi\Sigma_s \approx \text{constant}). \tag{14}$$

The spectrum emerging from small moderators is somewhat modified from this form,

$$\bar{i}(E, \boldsymbol{\Omega}_0) \propto 1/E^{1-\alpha}, \tag{15}$$

where α is a constant related to the neutron leakage probability. For a typical pulsed source moderator isolated from its surroundings, $\alpha \approx 0.15$.

6.3. The neutron pulse at low energies

At energies lower than about 1 eV the time distribution of the neutron pulse from moderators is of the form illustrated by fig. 7[13]). At highest energies the pulse rises and falls rapidly and is of the form of eq. (10). For energies $E_c \approx 5E_T$ and below, the pulse rises more slowly and peaks as neutrons thermalize in the medium and higher-than-fundamental modes of the neutron distribution decay. Following this peak, the pulse decays exponentially as $\exp(-\lambda_0 t)$, where λ_0 is the decay constant of the longest-lived fundamental mode. The fundamental mode energy distribution is of Maxwellian form $I_{MBo}(E_0) = (E/E_{TO}^2) \exp(-E/E_{TO}) I_{ThO}$, with different effective temperature E_{T0} than the time-integrated spectrum of eq. (7). For fig. 7, $\lambda_0 = 41$ s and $E_{T0} = 0.029$ eV while $E_T = 0.033$ eV. The pulse width depends in part on the rise time for thermalization, and in part on the fundamental mode decay constant. The full width at half maximum of the exponential decay is

$$\Delta t_0 = \ln 2/\lambda_0 .$$

λ_0 can be expressed in terms of the buckling expansion

$$\lambda_0 = \alpha_0 + D_0 B^2 - C B^4 + \ldots ,$$

where $\alpha_0 = \langle \upsilon \Sigma_a \rangle$ is the spectrum averaged absorption rate, $D_0 = \langle \upsilon D \rangle$ is the diffusion constant and C the diffusion cooling constant. Sjøstrand's[17]) values for these parameters in polyethylene are

$$\alpha_0 = 5900 \text{ s}^{-1}, \quad D_0 = 26\,600 \text{ cm}^2/\text{s},$$
$$C = 5900 \text{ cm}^4/\text{s}.$$

The expression (17) is accurate for not too large values of B^2. No discrete mode exists for very small moderators, and eq. (17) is meaningless.

6.4. The spectrum of neutrons at low energies

In moderators isolated from their surroundings, the spectrum of neutrons at low energies is that of a bare moderator. The spectrum is of different form in two energy ranges: for $E \lesssim 5E_T$, $\bar{I}(E)$ has the form of a Maxwellian flux distribution

$$\bar{I}_{MB}(E) = \bar{I}_{Th} \frac{E}{E_T^2} \exp(-E/E_T), \tag{18}$$

where $\bar{I}_{Th} = \int_0^\infty I_{MB}(E)\, dE$ is the total thermal neutron beam current, $E_T = k_B T$, and T is the characteristic temperature of the distribution. T is typically significantly greater than the physical temperature.

The shapes of spectra can conveniently be characterized by three parameters, the characteristic temperature, E_T, the ratio of total thermal neutron beam current to the beam current at 1 eV, $I_{Th}/E\bar{I}(E)|_{1\,eV}$ and the slowing-down spectral exponent α (although α is usually so small as to be of little interest in the narrow interval between E_c and 1 eV).

If $\alpha \approx 0$ and $I_{Th}/(EI(E)|_{1\,eV} \geq e^2/4$, the Maxwelli-

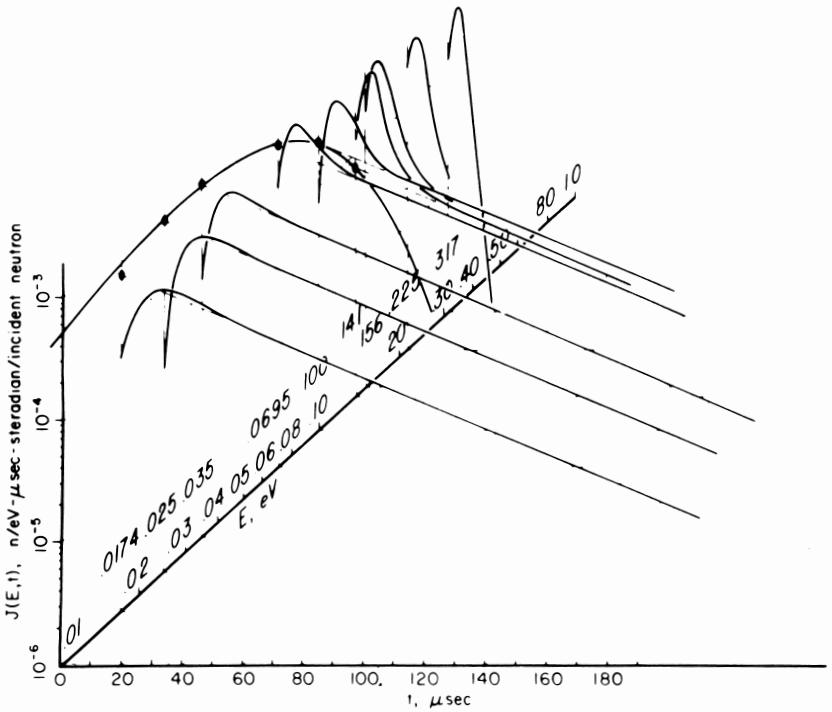

Fig. 7. Time dependent neutron spectra emerging from a 296 K polyethylene moderator ($\rho = 0.92$ g/cm^3, $3.83 \times 10 \times 10$ cm^3). Unpoisoned. On the $t = 0$ plane is shown the Maxwellian function fitted to the asymptotic decays[13].

an smoothy joins the slowing down distribution around an energy E_c given by

$$\left(\frac{E_c}{E_T}\right)^2 \exp(-E_c/E_T) = \frac{EI(E)|_{1\,eV}}{I_{Th}}. \tag{19}$$

$E_c \approx 5E_T$ when $I_{Th}/EI(E)|_{1\,eV} \approx 6$. Low energy spectra are difficult to compute (adequate cross section data exist for only a few materials) but measurements are available for an increasing number of cases. Fig. 8 shows a representative spectrum normalized to $EI(E)|_{1\,eV}$, measured at ZING-P (see below). Using the normalized spectrum the measured time average beam current is

$$\bar{i}(E) = \frac{I(E)}{EI(E)|_{1\,eV}} E\bar{I}(E)|_{1\,eV}\, \bar{S}_N. \tag{20}$$

$EI(E)|_{1\,eV}$ characterizes the source–moderator coupling, and can be obtained by calculation for a geometry including the particular moderator and source. Materials in the moderator which do not affect neutrons at high energies such as Cd, influence only $I_{Th}/EI(E)|_{1\,eV}$, not $EI(E)|_{1\,eV}$. $I_{Th}/EI(E)|_{1\,eV}$ can be obtained by calculation or measurement independently of the particular source. $\bar{S}_N$ is obtained for the source by calculation or by measurement.

An expression for $I_{Th}/EI(E)|_{1\,eV}$ for small homogeneous moderators, derived from age-diffusion theory is

$$I_{Th}/EI(E)|_{1\,eV} = \frac{\xi\Sigma s(1\,eV)}{\bar{\Sigma}_{a\,Th}(E_T)} \frac{D_{Th}(E_T)}{D(1\,eV)} \times \times \frac{\exp\{-B^2[\tau_{Th}(E_T) - \tau(1\,eV)]\}}{1 + L_{Th}^2 B^2}, \tag{21}$$

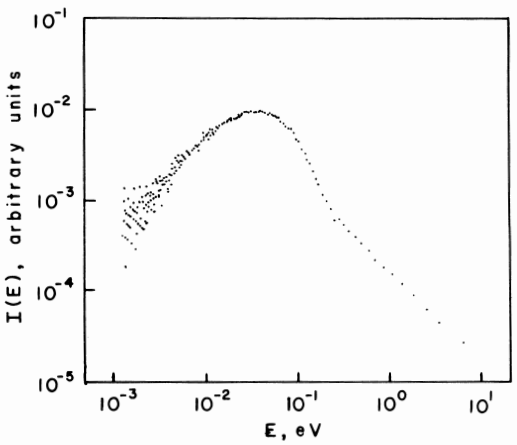

Fig. 8. Neutron spectrum for a 300 K $10 \times 10 \times 2$ cm^3 CH_2 moderator measured at the ZING Prototype.

where $\bar{\Sigma}_{a\,Th}(E_T)$ and $D_{Th}(E_T)$ are the thermal spectrum averaged absorption cross section and diffusion coefficient, $D(1\text{ eV})$ is the diffusion coefficient at 1 eV, $L^2_{Th} = D_{Th}/\bar{\Sigma}_{a\,Th}$ is the thermal diffusion length, $\tau_{Th}(E_T)$ and $\tau(1\text{ eV})$ are the Fermi age to thermal and to 1 eV respectively, and B^2 is the geometric buckling of the moderator. For a $10 \times 10 \times 5$ cm^3 CH_2 moderator with $E_T = 0.035$ eV and $\rho = 0.94$ g/cm^3, using ENDF-BIII cross sections for CH_2, eq. (21) gives

$$I_{Th}/EI(E)|_{1\,eV} = 5.3,$$

in close agreement with measurements.

In very large moderators such as the slow neutron source regions of steady state reactors,

$$I_{Th}/EI(E)|_{1\,eV} = \xi\Sigma_s/\bar{\Sigma}_{a\,Th}, \qquad (22)$$

where $\xi\Sigma_s/\Sigma_{a\,Th}$ is the "moderating ratio". Table 8 gives the moderating ratio for a number of materials.

Small hydrogeneous moderators are relatively inefficient compared to D_2O and Be in providing high thermal neutron fluxes in relation to the number of neutrons slowing down. They are preferred for pulsed moderators because they provide short pulses. It is possible to produce sufficiently intense pulsed fast sources, so that when the peak thermal neutron flux is comparable with that in steady state reactors, the flux of epithermal neutrons is

TABLE 8

Moderating ratios of some moderator materials.

Material	Temperature (K)	$\xi\Sigma_s(1\text{ eV})/\bar{\Sigma}_{a\,Th}$
H_2O	300	70
D_2O (99.8 at. %)	300	2 500
Be	300	140
D_2 (99.8 at. %)	20	250
C	2 000	500

TABLE 9

Spectral parameters of some moderators.

Material	T(K)	Dimensions	Cd depth	E_t	$I_{Th}/EI(E)\|_{1\,eV\,(ref.)}$
CH_2	300	10×10×5.1	–	0.035	5.6
CH_2	296	10×10×3.82	–	0.0325	4.3
CH_2	296	10×10×5.1	0.63	0.0422[a]	0.43[a]
				0.036[a]	0.36[a]
CH_2	296	10×10×5.1	1.00	0.037	0.90
CH_2	296	10×10×5.1	1.3	0.036	1.4
CH_2	296	10×10×5.1	2.55	0.033	3.5
CH_2	296	10×10×7.65	1.00	0.037	0.92
CH_2	296	10×10×7.65	2.55	0.034	3.6
CH_2	77	10×10×7.65	–	0.0084	3.8
CH_2	77	10×10×7.65	2.55	0.0096	2.7
CH_4	77	10×10×7.65	–	0.0090	5.9
NH_3	77	10×10×7.65	–	0.0106	2.6
CH_2	300	12×25×4.4	–	0.035	
CH_2	77	12×25×4.4	–	0.011	
CH_2	4	12×25×4.4	–	0.0065	
H_2O	300	12×25×5	–	0.038	
H_2O	77	12×25×5	–	0.010	
H_2O	4	12×25×5	–	0.0063	
P-H_2	20.4	14.80×16	–	0.004	7.6
H_2	18	20 dia×20[b]	–	0.003	3.3
C_9H_{12}	21.4	20 dia×20[b]	–	0.003	9.0
C_2H_6	182	20 dia×20[b]	–	0.025	7.5
C_2H_6	20.2	20 dia×20[b]	–	0.004	5.9
CH_4	77	20 dia×20[b]	–	0.01	16.3
CH_4	20	20 dia×20[b]	–	0.0025	6.1

[a] In this very thin moderator, no equilibrium spectrum is developed, so the Maxwellian parameters are not well determined.
[b] Measured through re-entrant hole.

several orders of magnitude greater than in steady sources.

Table 9 gives spectral parameters of a number of moderators. Spectra are shown in figs. 9 and 10, which represent the effects on the spectrum of changing size through heterogeneous poisoning by cadmium[13]) and of cooling condensed methane[15]). Measurements through re-entrant holes in moderators such as those cited above for methane are only approximately valid for applications in which a large outer surface is viewed. The effects of heterogeneous poisoning and of cooling on the effective temperatures are shown in figs. 11 and 12. Homogeneously added absorbers lead to higher effective temperatures and lower intensities. Materials in which the protons participate with large amplitudes in low frequency motions thermalize neutrons more efficiently than those with tightly bound protons – the distribution of frequencies influences the spectrum.

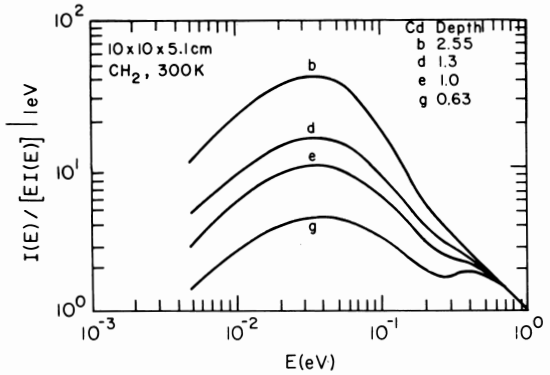

Fig. 9. Slow neutron spectra for heterogeneously poisoned 300 K polyethylene moderators $10 \times 10 \times 5.1$ cm^3, with 0.05 cm cadmium various depths beneath the viewed surface[13]).

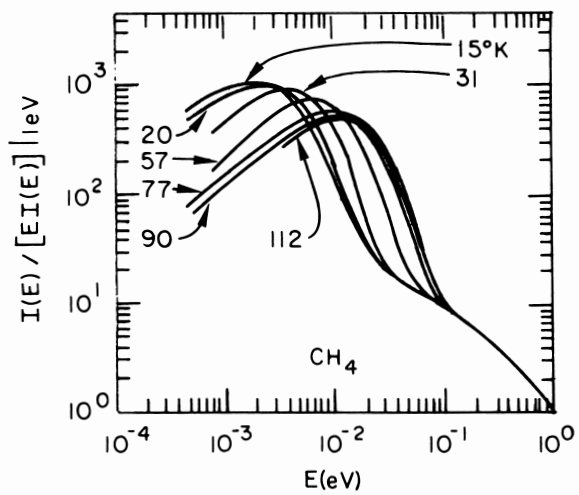

Fig. 10. Slow neutron spectra measured through a reentrant hole in 20 cm diam. × 20 cm high methane moderators as a function of temperature[18]).

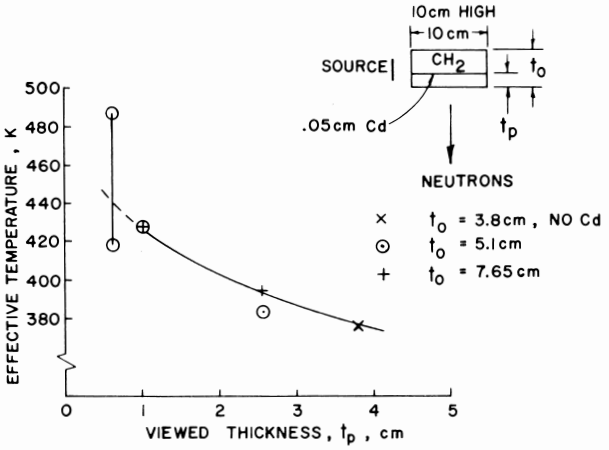

Fig. 11. Effective temperature and thermal to epithermal flux ratio for heterogeneously poisoned 300 K $10 \times 10 \times 5.1$ cm^3 polyethylene moderators[13]).

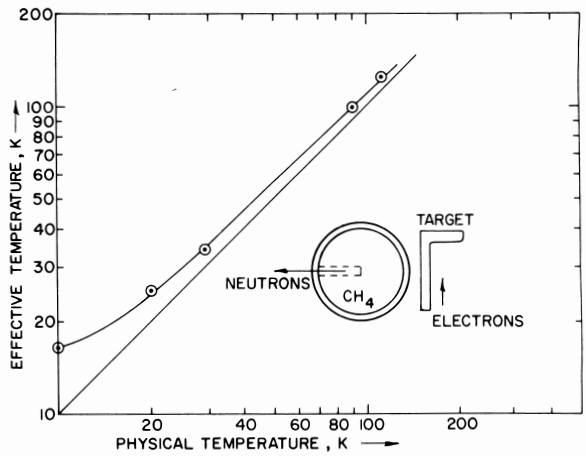

Fig. 12. Effective temperature and thermal to epithermal flux ratio for 20 cm diam. × 20 cm high methane moderators[18]).

6.5. Pulse widths at low energies

The effects of heterogeneous poisoning on the pulse width in polyethylene moderators is illustrated in fig. 13 for some of the moderators studied by Graham[13]) for which the thermal neutron spectrum parameters were given above. While the pulse width is narrower for small moderators, the figure of merit $\int I(E, t)\,dt/\tau^2$ is only a mild function of poison depth, peaking between 1 and 2 cm. The same effects due to heterogeneous and homo-

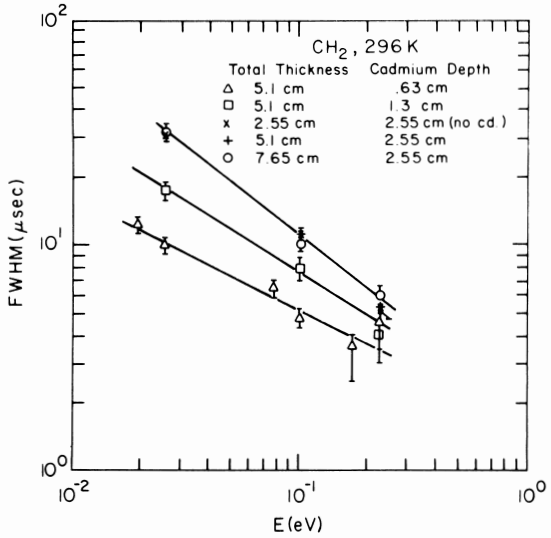

Fig. 13. Pulse widths for heterogeneously poisoned 300 K polyethylene moderators $10 \times 10 \times 5.1$ cm^3, with 0.05 cm cadmium various depths beneath the viewed surface[18]).

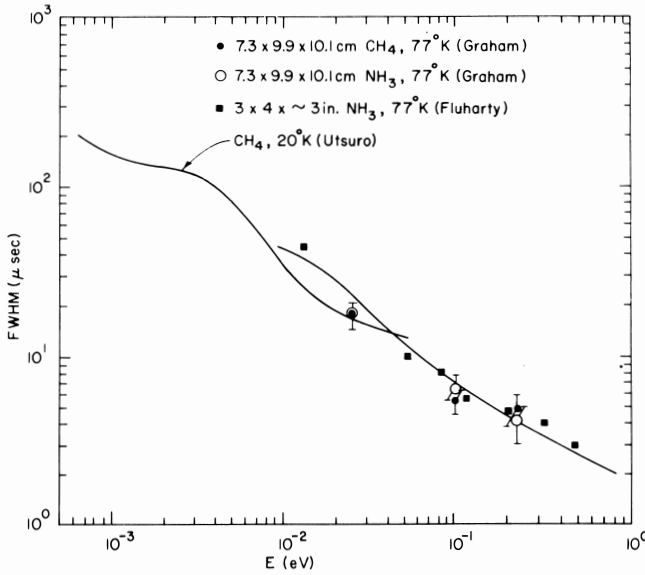

Fig. 14. Pulse widths for methane and ammonia moderators as a function of temperature[13,17,18]).

geneous poisoning are further illustrated by the data of Watanabe et al.[16]).

The effect of cooling methane moderators and the comparison of pulse widths of methane and ammonia moderators is illustrated in fig. 14 on the basis of data of Graham[11]), Fluharty et al.[17]) and Utsuro et al.[18]). Methane and ammonia provide approximately the same pulse widths at 77 K. 20 K methane provides shorter pulses in the range around 0.01 eV than 77 K methane, but at energies below 0.01 the data suggest that pulses are shorter for the *warmer* moderator. This last effect has also been demonstrated in the data of Ishmaev et al.[19]).

6.6. Emission time delays

It is essential with regard to time-of-flight instrument calibration and accurate spectrum measurements, to note that the mean time of emission of the pulse $\bar{t}$ is not constant with energy nor does it represent a constant distance shift. Fig. 15 shows data from Graham's measurements on heterogeneously poisoned polyethylene moderators plotted as $v\bar{t}$ vs neutron energy. For the thickest moderator, $v\bar{t}$ is as large as 15 cm at 0.1 eV, then decreases to 2–3 cm at energies of a few tenths eV and above. For the thinnest moderators $v\bar{t}$ is nearly constant, and equal to 2 or 3 cm. The infinite medium value from eq. (11) is 1.8 cm at 1 eV. The curves are estimates of the trends in the data, which show considerable scatter.

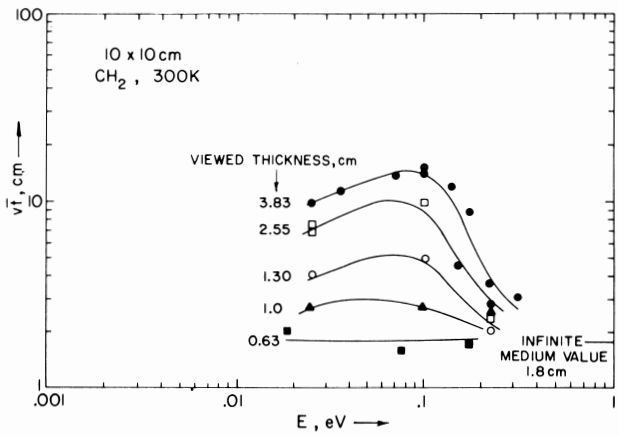

Fig. 15. Emission time delays for heterogeneously poisoned 300 K polyethylene moderators $10 \times 10 \times 5.1$ cm^3, with 0.05 cm cadmium various depths beneath the viewed surface[13]).

6.7. Source-moderator coupling, slowing-down leakage losses, and reflectors

Since $EI(E, \boldsymbol{\Omega}_0)$ is approximately constant for $E \gtrsim 1$ eV and up to energies at which source neutrons are generated, $EI(E, \boldsymbol{\Omega}_0)|_{1\,\mathrm{eV}}$ is a convenient quantity in terms of which to express the source-moderator coupling efficiency. For example for a polyethylene moderator $10 \times 10 \times 5$ cm^3, 6.75 cm from a source, the results of Graham[11]) can be interpreted to give $EI(E)|_{1\,\mathrm{eV}} \sim 4.3 \times 10^{-5}$ n/sr·source neutron. Graham's measurements included the

reflecting effect of a 2.54 cm layer of natural B_4C around the moderator, which he found enhanced the emerging beam current by about $\times 2$ above that for an unreflected moderator. The coupling of Graham's 14 MeV source was less efficient than would be that of a source of ~ 1 MeV neutrons, so 4×10^{-5} n/sr·source neutron roughly represents the coupling of an unreflected moderator to a ~ 1 MeV neutron source.

Losses in slowing down are very substantial and can be estimated as follows. Since $EI(E).E^{a}$ (1 eV $\lesssim E \lesssim$ 1 MeV), the ratio of beam currents at 1 eV with and without leakage, is

$$\left(\frac{1\text{ eV}}{10^{6}\text{ eV}}\right)^{x} \cong (10^{-6})^{0.15} = 0.13.$$

This leakage loss can be very considerably reduced by surrounding the moderator with reflector. Experiments on an arrangement called the "ZING Mockup" at Argonne[20]) indicated that with a beryllium reflector around a $10 \times 10 \times 5$ cm^3 polyethylene moderator, $I_{\mathrm{Th}} = 4.3 \times 10^{-3} \pm 4\%$ n/sr·source neutron. Since for this moderator the ratio $I_{\mathrm{Th}}/EI(E)|_{1\,\mathrm{eV}} = 5.6$ was determined in measurements at ZING-P (see below and fig. 17), in the ZING-Mockup,
$EI(E)|_{1\,\mathrm{eV}} = I_{\mathrm{Th}}/[T_{\mathrm{Th}}/(E)|_{1\,\mathrm{eV}}] = 7.7 \times 10^{-4}$ n/sr·n$_s$,
indicating more than a 10-fold improvement over the bare moderator result.

The moderator-reflector works to reflect back those neutrons which collided first in the moderator but would have leaked out in slowing down and also enables neutrons which would have missed the moderator to migrate to it, slow down and emerge in the direction of interest. In addition (n, 2n) reactions induced above 1.7 MeV in Be enhance the number of neutrons available. Calculations indicate that this effect increases the beam current by about 25% in a spallation neutron source.

Das et al.[21]) and Russel et al.[22]) have made extensive calculations of the source-moderator coupling efficiency, and of the time and energy dependence of the neutron beam currents for numerous target and moderator materials and configurations. Calculations of Das for the ZING-Mockup arrangement gave $EI(E)|_{1\,\mathrm{eV}} = 7.9 \times 10^{-4}$ n/sr·source neutron, in agreement with the measurement. Russel's calculations of the ZING-Mockup also verify the intensity gain due to the Be reflector.

The reflector broadens the slow neutron pulse from the moderator somewhat. In order to prevent neutrons which thermalize in the Be reflector from entering the moderator after long times, it is necessary to decouple the moderator from the reflector by a layer of material which absorbs neutrons at thermal energies. Cadmium decouples at about 0.5 eV; a layer containing $N_{10\mathrm{B}}$ Boron-10 atoms/cm^2 attenuates neutrons of energy E by a factor
$\exp[-N_{10\mathrm{B}}\,\sigma_a(E)] = \exp[-6.04 \times 10^{-22}\,N_{10\mathrm{B}}/\sqrt{E(\mathrm{eV})}]$
and decouples roughly at

$$E_{\mathrm{d}} = (6.04 \times 10^{-22}\,N_{10\mathrm{B}})^{2}\ \mathrm{eV}. \qquad (23)$$

Decoupling limits the reflecting effect to energies above the decoupling energy. The excess pulse broadening which occurs due to the reflector above E_{d} persists as a constant broadening in excess of the bare moderator pulse width at lower energies.

Reflectors broaden the pulse beyond the value for the bare moderator. If the reflector is decoupled at an energy greater than about 0.5 eV, the effect on the pulse at low energies is small and the added intensity comes with negligible penalty in pulse width. There is no simple theory

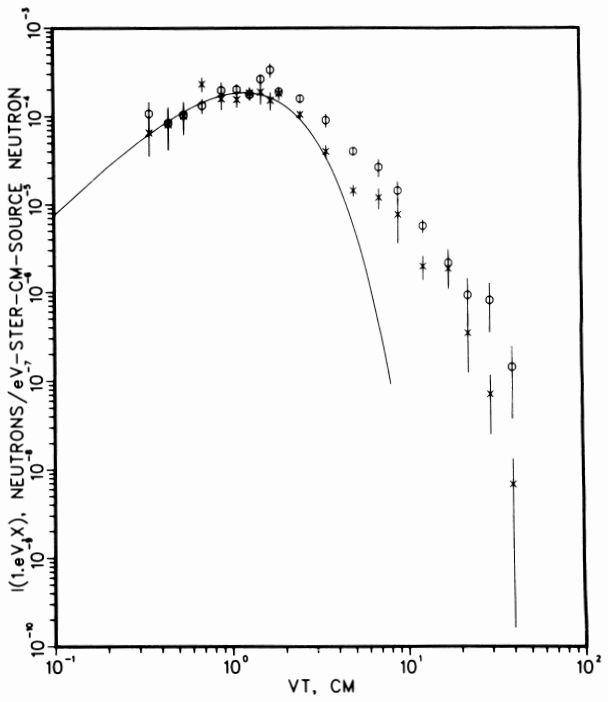

Fig. 16. Beam intensity at 1 eV as a function of time (expressed as a function of $x = vt$) for the ZING Mockup (see text). ○ No boron liner; × with boron liner in beam hole void only. Solid line is for an infinite medium of polyethylene [eq. (10)][21]).

by which to estimate the reflector broadening, which may be important at energies above a few tenths eV. Das[21]) has computed the detailed time distribution as a function of energy for the ZING-Mockup, a $10\times10\times5$ cm^3 CH_2 moderator with a beryllium reflector and a 10×10 cm^2 beam hole. She calculated two cases:

a) Cadmium decoupling only (ignored in calculations above 1 eV).
b) Boron liner inside the beam hole void only (moderator decoupled by cadmium).

Her results for 1 eV neutrons are shown in fig. 16. Russel[14]) has also computed the moments of the time distribution for the same case, but not the detailed shape. The moments determined in both calculations at 1 eV are shown in table 10. Expressed in terms of vt rather than t, these results are almost independent of energy, as are the pulse shapes.

The moments are consistent in the two calculations for case (a), and for both cases significantly greater than the values for the bare moderator, table 7. This is due to the long tail on the distribution, which is significantly suppressed by the boron liner, and is therefore partly due to streaming across the beam hole void. Also plotted in the figure is the bare moderator pulse shape calculated by eq. (5), arbitrarily normalized. Comparison of the bare moderator pulse shape with that for case (b) indicates the very important result that the reflector broadens the pulse little if any near the peak, but adds a tail which increases $\bar{t}$ and σ_t.

6.8. Effective peak flux

A quantity useful for characterizing pulses sources is the "effective peak flux" at the moderator surface

$$\hat{\phi}_{\mathrm{eff}}(E) = \frac{4\pi\bar{i}(E)}{Af\tau(E)} = \frac{4\pi}{Af\tau(E)}\left[\frac{I(E)}{EI(E)|_{1\,\mathrm{eV}}}\right]\times \times E\bar{I}(E)|_{1\,\mathrm{eV}}\,\bar{S}_{\mathrm{N}}. \quad (24)$$

$\hat{\phi}(E)$ can be interpreted as the equivalent isotropic flux averaged over the moderator surface which is reached during a pulse of width τ. Of course the flux is neither isotropic nor uniformly distributed across the moderator surface, nor is the pulse of simple shape. Nevertheless, if the intensity in a neutron beam is computed from $\hat{\phi}(E)$ for a pulsed source as one would do for a reactor source, the correct result is produced. For less detailed characterization an "effective peak thermal neutron flux"

$$\hat{\phi}_{\mathrm{Th\,eff}} = \frac{4\pi\bar{i}_{\mathrm{Th}}}{Af\tau} = \frac{4\pi}{Af\tau}\left[\frac{I_{\mathrm{Th}}}{EI(E)|_{1\,\mathrm{eV}}}\right] EI(E)|_{1\,\mathrm{eV}}\,\bar{S}_{\mathrm{N}} \quad (25)$$

is useful with τ chosen at the energy of a typical experiment. In this paper $\tau = \tau(0.05\ \mathrm{eV})$.

7. Moderator materials

Materials to be used as pulsed moderators must withstand irradiation and both ambient temperature and cryogenic moderators must be cooled in addition to having high proton densities and efficient energy-loss mechanisms. Polymers degrade under irradiation but are useful as moderators at doses far beyond those which degrade mechanical properties. Some irradiated moderators have exploded after warming from low temperature irradiation due to hydrogen gas buildup or Wigner effect. Flowing liquids offer easy means of heat removal, however solids of higher molecular weight are formed in irradiated light hydrocarbons which may clog piping. Liquid hydrogen, ammonia and water do not form solid products under irradiation, but consideration must be given to evolved toxic and flammable gases. Some metal hydrides have high proton densities and are resistant to radiation damage.

Mildner[23]) has reviewed relevant neutron thermalization thermal and radiation damage properties (as relate to photon damage) of some possible cryogenic moderators. His data are reproduced in

Table 10
Pulse shape parameters for ZING-Mockup calculations.

Case	$EI(E)\|_{1\,\mathrm{eV}}$ (n/sr·n$_s$)	vt (cm)	$v\sigma_t$ (cm)	$v\tau$ (cm)	
(a) No boron	7.9×10^{-4}	3.9	4.6	2.2 (Das)	($\rho = 0.04$ g/cm^3)
		4.0	4.8	— (Russel)	($\rho = 0.90$ g/cm^3)
(b) Boron void liner	5.1×10^{-4}	3.0	3.5	1.9 (Das)	
Infinite moderator		1.82	1.03	2.00	

TABLE 11

Properties of some cryogenic moderator materials.

	Hydrogen atom density of N_H (Å^{-3})	Melting point (K)	Boiling point (K)	Low energy exchange modes (eV)	Radiation damage[a]
1) H_2	0.042	liquid	20.4	0.015	–
2) C_9H_{12}	0.052	220	438	0.0074	–
3) H_2O	0.067	273		none	0.43
4) CH_4	0.078	90	112	0.017	22.2
5) $(CH_2)_n$	0.079	solid		none	13.2
6) NH_3	0.088	195	240	0.0025	4.4

[a] cm^3 of total gas evolved at normal temperatures and pressures per cm^2 of 5 cm thick moderator at a distance of 10 cm from the source, for electron and photon irradiation.

table 11. Vetrano[24]) has reviewed the properties of some metal hydrides as they relate to use as moderator materials in reactors. The hydrides provide high proton densities and are tolerant of high doses and high temperatures, but the protons are tightly bound and participate little in low frequency motions.

Coolants for cryogenic moderators must exhibit adequate stability under irradiation, and be able to carry off the required heat. Mildner[23]) has compiled a table of the properties of some cryogenic coolants which is reproduced in part as table 12.

The low temperature provided by liquid He may not be required, since spectral temperatures are not lowered much below 20 K even at lower physical temperatures. Cold He gas is attractive and applicable to all temperatures of interest. Liquid hydrogen seems attractive from nearly all points of view except flammability. Liquid neon, with almost as low a boiling temperature as hydrogen lacks this drawbback. Liquid nitrogen, irradiated in the presence of oxygen has been known to explode and has a significant neutron absorption cross section, but is a convenient coolant. Argon has nearly as low a boiling temperature as N_2 and lacks the drawbacks of nitrogen.

Heating and radiation damage in moderators adjacent to spallation neutron sources is predominantly due to neutrons. This is distinct from the case of electron linac photoneutron sources, at which the heating and damage is primarily due to photons and electrons. Taking the energy distribution of neutrons to be that emerging from a ^{238}U target at 90° from an 800 MeV proton beam[4]) the average energy is 4 MeV and the average flux-to-dose conversion factor[5]) is $3.5 \times \times 10^{-9}$ Rad/(n/cm^2). For example, for a source producing 9×10^{16} n/s, the dose rate 6 cm from the source is 700 kRad/s and the energy flux is 128 W/cm^2. The total thermal power which must be dissipated from a $10 \times 10 \times 5$ cm^3 moderator with 5×10 cm^2 facing the target is 6 kW. These dose and heating rates are similar to those encountered in nuclear power reactors and dictate careful consideration of radiation damage and cooling requirements and probably restrict moderator choice to flowing systems of H_2O, NH_3, CH_4, H_2 etc. and to metal hydrides.

TABLE 12

Properties of some cryogenic coolants.

Refrigerant	Boiling temperature at 1 atm (K)	Max. nucleate boiling heat flux (W/cm^2)	Specific heat of vapor (cal/g·mol °C)	Heat of vaporization (cal/cm·mol)
N_2	77.	20.	7.3	1 330
N_e	27.	6.	5	414
H_2	21.	9.	5.7	213
He	4.2	0.6	5.	19.4
Ar	87.		5.	1 560

TABLE 13
ANL pulsed neutron source program.

Facility	Proton accelerator	Protons/ pulse	Proton energy (MeV) and target	No. of neutron beams	Neutrons/ proton	Frequency (c/s)	Peak thermal neutron flux ($n/cm^2 \cdot s$)	Operation
ZING-P	ZGS Booster I	2.5×10^{10}	200 Pb	2	2	10	5×10^{11}	January 1974
ZING-P′	ZGS Booster II	1×10^{12}	500 W	4	8	30	1×10^{14}	March 1977
PPNS	ZGS Booster II	5×10^{12}	500 ^{238}U	6	20	30	1.2×10^{15}	August 1979
IPNS	HIS[a]	5×10^{13}	800 ^{238}U	12	30	60	10^{16}	October 1983

[a] High Intensity Synchrotron.

8. The ZING-Prototype

In the fall of 1973, a small-scale neutron source was constructed based on the 200 MeV Booster I proton synchrotron of the 12.5 GeV Zero Gradient Synchrotron (ZGS) accelerator system at Argonne National Laboratory. Neutrons were produced by the spallation process in a target of lead. The neutron source was designed to produce pulsed neutron beams for slow neutron scattering research, as a prototype of a large scale facility, called ZING (*Z*GS *I*ntense *N*eutron *G*enerator). ZING was to have been a neutron source based on the 500 MeV Booster II proton synchrotron. The prototype was called the ZING Prototype, ZING-P. Efforts are now being devoted toward a facility with higher performance, called *I*ntense *P*ulsed *N*eutron *S*ource (IPNS), which will produce peak thermal neutron fluxes of 1×10^{16} $n/cm^2 \cdot s$ at 60 Hz and time average fast neutron fluxes of 3×10^{14} $n/cm^2 \cdot s$. The IPNS will be based on a new, dedicated, High Intensity Synchrotron[7]). Various stages in the ANL pulsed neutron source development program including the intermediate prototypes ZING-P′ and PPNS, are described in table 13. The ZING-P neutron source was operated during three roughly one-month periods in Feb. 1974, Sept. 1974 and Feb. 1975. This was the first demonstration of a spallation neutron source

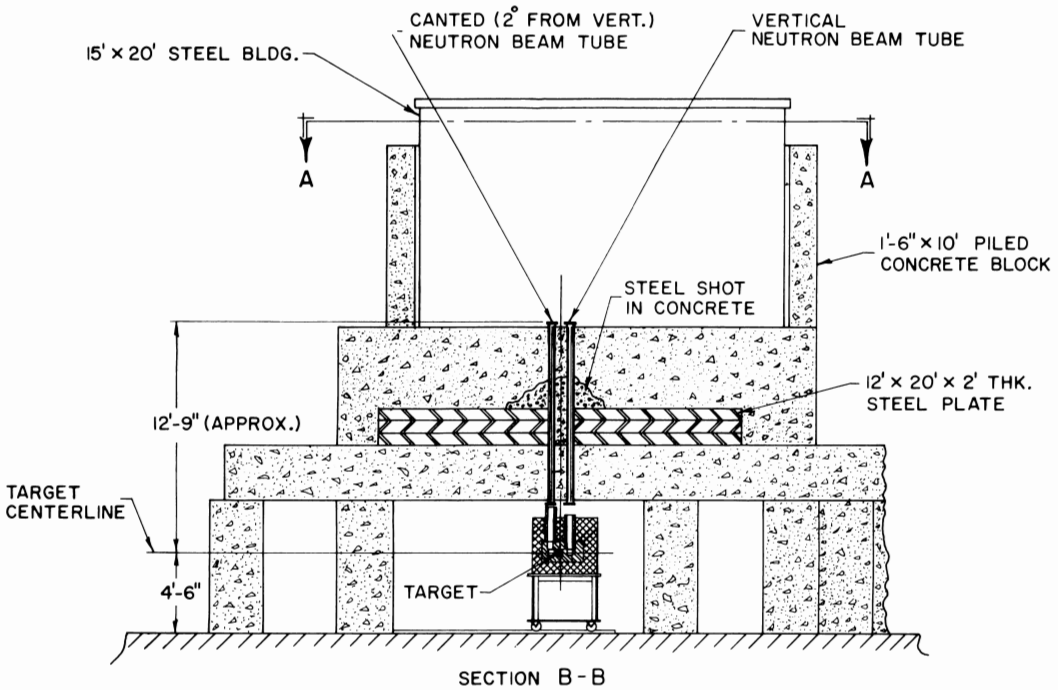

Fig. 17. Cross section through the ZING Prototype facility. Protons strike the target from behind this view.

for slow neutron scattering studies. A more complete description of the instruments and some results has appeared elsewhere[25]).

8.1. Booster I accelerator

The "Booster I" accelerator was the former 2 GeV Cornell electron synchrotron reincarnated as a proton synchrotron to serve as a test bed for development of the ZGS Booster II[9]). H^- ions were accelerated to 50 MeV in the ZGS proton linac, and injected into the synchrotron by stripping, then accelerated to a final energy of 200 MeV. The space charge limit was calculated to be 6×10^{11} protons/pulse. Protons were extracted in a single turn, in a pulse 100 ns in duration. The accelerator was designed to operate at a frequency up to 30 Hz. During the operation of ZING-P, Booster I delivered on the average about 2.5×10^{10} protons/pulse at 10 Hz. This amounts to an average current of 0.04 μA and an average beam power of 8 W.

8.2. The neutron source

In the shielded tunnel connecting Booster I to the ZGS, a neutron-producing target assembly was erected, as shown in figs. 17 and 18. The target was of Pb, 6.4 cm × 10.2 cm, 7.6 cm thick. (The range of 200 MeV protons in Pb is 4.8 cm.) The spallation neutron yield for 200 MeV protons in Pb is approximately 2 n/p, but not well known. Two 300 K polyethylene moderators, 10 cm × × 10 cm × 5 cm, were placed adjacent to the Pb source and on opposite sides. These were viewed through two beam holes, one vertical and the other inclined 2° off vertical to provide clearance between the exiting beams.

The dimensions and inclinations of the moderators relative to the beam direction were varied during the measurements to provide optimum pulse widths and orientations for time focusing.

Surrounding the moderators and source was a reflector of Be metal, which in turn was surrounded by a layer of Pb bricks for shielding. Bor-

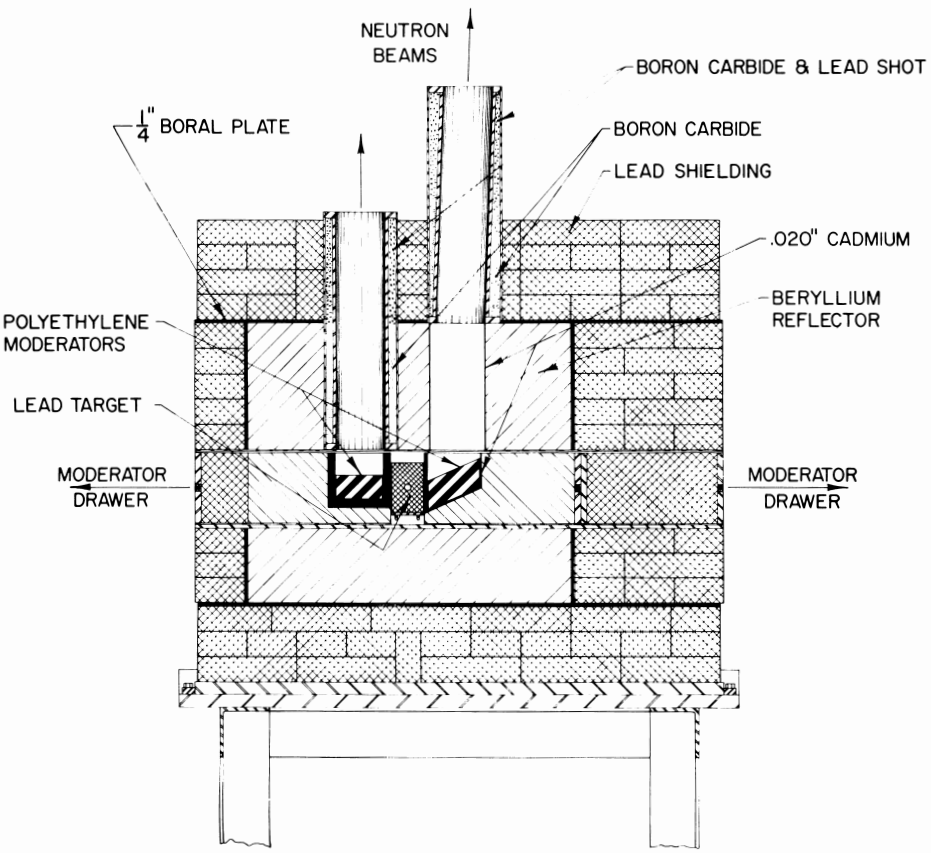

Fig. 18. Cross section through the ZING Prototype target–moderator assembly. Lead shielding bricks 5.1 × 10.2 × 20.3 cm^3 give scale to the figure.

al plates were placed between the Be and the Pb shielding to reduce activation by thermal neutrons, and to reduce the possibility of pulse broadening by room return or the return of neutrons slowing down in Pb. The Pb neutron source and the two moderators were arranged to slide in drawers within a T-shaped tunnel, an arrangement which was found to be very convenient when changes were to be made in the moderators.

The vertical beam moderator was designed for producing short pulses, and was surrounded, except on the emerging surface, by a 2.54 cm thick layer of B_4C epoxy, which contained 3.6×10^{22} $^{10}B/cm^2$. This decoupled the moderator from the reflector at all energies below 500 eV so that the reflector broadening was insignificant. Recent calculations indicate that decoupling at such high energies is not necessary. The moderator was heterogeneously poisoned with a 0.5 mm layer of Cd placed 1.27 cm beneath the emerging surface.

The slanted beam moderator was designed for applications requiring highest intensity, and was surrounded, except on the emerging surface, by a 0.5 mm layer of Cd, which decoupled it from the reflector at all energies below about 0.5 eV.

The pulse full width at half-maximum $\tau(E)$ is shown in fig. 19 as a function of neutron energy. For the boron-decoupled (vertical beam) moderator, results are taken from ref. 13. For the Cd decoupled (slanted beam) moderator, pulse widths were measured during ZING-P operation at various energies using a crystal spectrometer whose resolution was calculated to be negligible except at the highest energy. Errors not shown are smaller than the plotting symbols.

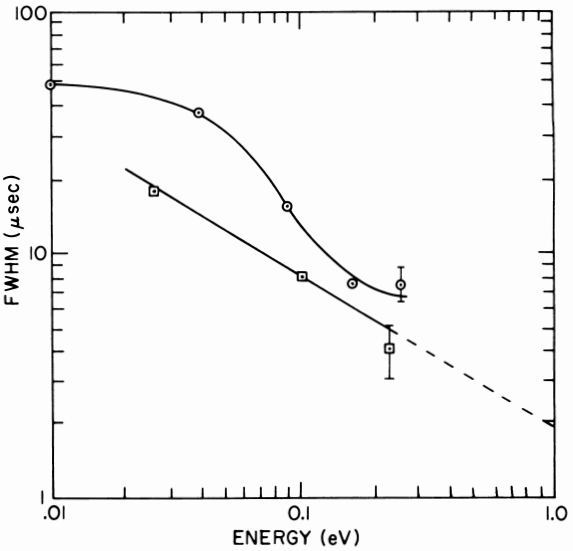

Fig. 19. Full width at half-maximum vs energy for ZING Prototype moderators. (a) Diffractometer (vertical beam) moderator. The moderator is heterogeneously poisoned by 0.5 mm Cd, 1.3 cm beneath the viewed surface. (b) The inelastic scattering (slanted beam) moderator. Measurements described in the text.

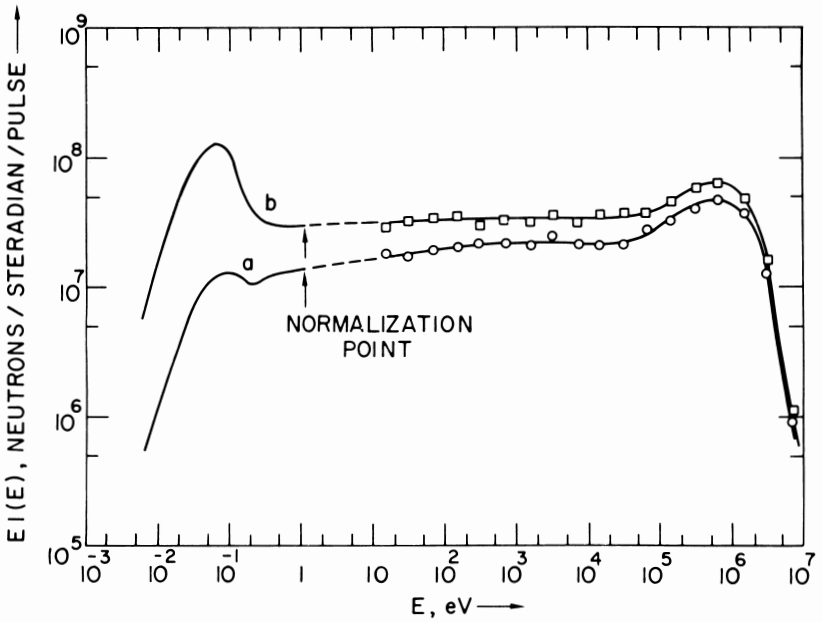

Fig. 20. Spectra of neutrons from the ZING Prototype moderators. (a) Diffractometer (vertical beam) moderator. (b) Inelastic scattering (slanted beam) moderator.

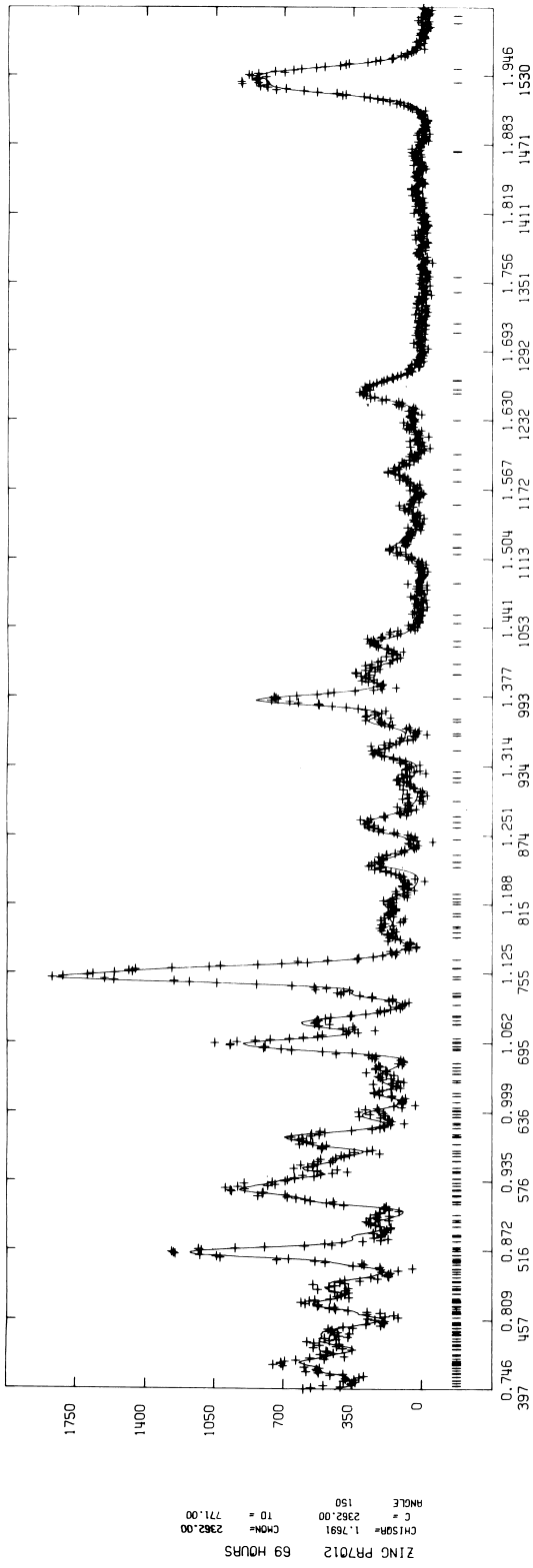

Fig. 21. Diffraction pattern of Pr_7O_{12} powder measured at ZING-P. The solid line is a profile fit using the function of Jorgensen[25]). Dashes represent the fitted reflections.

Fig. 20 shows the beam current per pulse $Ei(E)$ normalized to calculations of Das[21]) using 2.5×10^{10} protons/pulse, 2 neutrons/proton.

Two instruments were operated at ZING-P. A time-focussed powder diffractometer with incident and scattered neutron paths 4.34 and 4.6 m and scattering angle $2\theta = 150°$ with detectors subtending 0.2 sr solid angle was erected at the vertical beam. The resolution $\Delta Q/Q \approx 0.01$ for all Q, and the instrument provided useful data for $3 \lesssim Q \lesssim 40$ Å^{-1}. A more complete description of the instrument was given in ref. 25 with examples of some results. Recently the measurement on Pr_7O_{12} has been analyzed with the result shown in fig. 21. The profile refinement of 463 lines in the data $0.75 < d < 2$ Å resulted in a fit of the two lattice constants and 9 atomic position coordinates with $\chi^2_R = 1.77$, using Jorgensen's line shape function[25]). The crystal analyzer spectrometer operated at the ZING-P slanted beam, with some illustrative results is described elsewhere in this issue[26]).

The successful results on admittedly carefully chosen experiments demonstrate the effectiveness of pulsed spallation neutron sources for neutron diffraction and neutron spectroscopy and their great potential when they are developed to their ultimate performance.

9. Argonne's intense pulsed neutron source

Argonne has proposed to construct the Intense Pulsed Neutron Source (IPNS)[27]) which is an example of the performance which can be obtained in pulsed spallation neutron sources. IPNS is based upon the High Intensity Synchrotron, an 800 MeV rapid cycling proton synchrotron of 20.3 m average radius operating at 60 Hz and having space charge limit of 5×10^{13} protons/pulse. H^- ions from a linear accelerator will be injected at 70 MeV by stripping in a thin foil. Single turn extraction will provide a proton pulse 250 ns long. A NaK-cooled ^{238}U target will produce 30 n/p so that the average neutron production rate is $\bar{S}_N = 9 \times 10^{16}$ n/s. Three differently tailored hydrogenous 10×10 cm^2 moderators surrounding the target will provide slow neutron beams to twelve beam holes. The proton beam will be shared with a radiation effects facility.

Fig. 22 shows the IPNS slow neutron target and moderator assembly. Calculations by Das for 2″ CH_2 moderators in this arrangement are given in table 14.

For moderator C with 0.05 cm Cd 2.55 cm be-

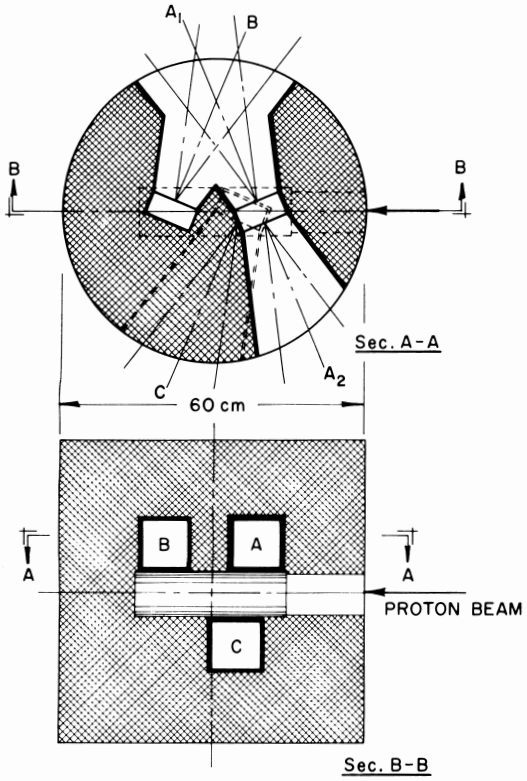

Fig. 22. The target, moderator, reflector assembly of the IPNS Neutron Scattering Facility. The proton beam enters horizontally, and impinges on the NaK-cooled target. Close by the target are three moderators, two above, and one below. All moderators are taken for the purposes of this conceptual design to be 10 cm × 10 cm and 5 cm thick, of CH_2 (which is nearly equivalent to H_2O). Moderator A is surrounded on its four 5 cm × 10 cm faces by a layer of $B_4^{10}C$, 0.5 cm thick, taken to have a density of 1.6 g/cm^3 and the beam openings are lined with a similar layer.

low the viewed surface and $I_{Th}/EI(E)|_{1\,eV} = 3.5$ and $\tau = \tau(0.05\,eV) = 30\,\mu s$, the effective peak thermal neutron flux will be $\hat{\phi}_{Th} = 10^{16}$ n/cm^2·s. Fig. 23 shows the effective peak flux per unit energy and the pulse width for the same moderator, compared with the flux spectra for the ambient and hot sources at the ILL reactor.

TABLE 14

IPNS moderator beam currents.

Moderator	$EI(E)\|_{1\,eV}$
A_1	2.8×10^{-4}
A_2	2.5×10^{-4}
B	2.5×10^{-4}
C	4.5×10^{-4}

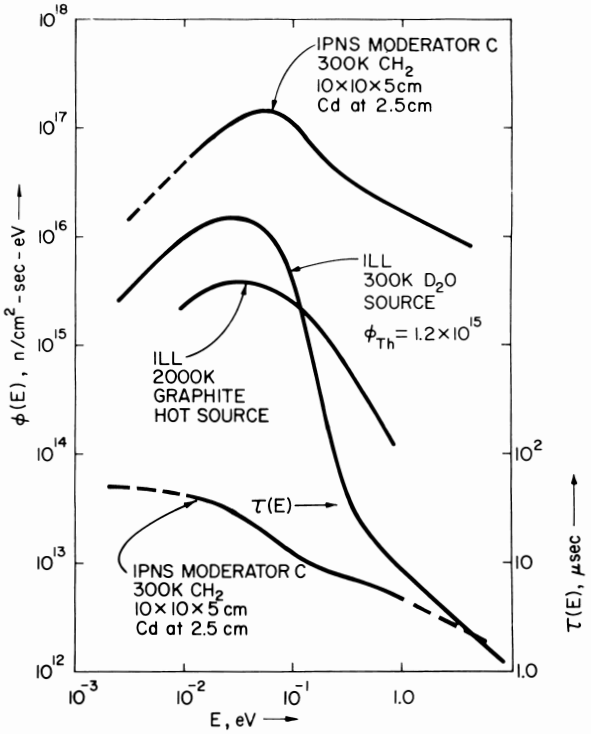

Fig. 23. Effective peak flux and pulse width for IPNS reference moderator C. The spectra for the ILL ambient temperature D_2O source and the 2000 K graphite hot source are shown for comparison.

10. Conclusion

Pulsed spallation neutron sources are a new generation of sources for slow neutron spectroscopy. The much increased thermal neutron fluxes and the unprecedently higher epithermal neutron fluxes which they offer will relieve the limitations on many classes of measurements which now exist and open up unique new areas for investigation.

References

[1] Proc. Conf. on *Neutron scattering*, Gatlinburg, Tennessee, USA CONF-760601-P1 (1976).
[2] R. M. Brugger, Phys. Today **21** (1968) 23.
[3] J. S. Fraser, R. E. Green, J. W. Hilborn, J. C. D. Milton, W. A. Gibson, E. E. Gross and A. Zucker, Phys. Canada **21** (2) (1965) 17; G. A. Bartholomew and P. R. Tunnicliffe (Eds.) AECL-2600 (Chalk River) (1966) p. VII, 12.
[4] R. R. Fullwood, J. D. Cramer, R. A. Harman, R. P. Forrest, Jr. and R. G. Schrandt, LA-4789 (Los Alamos Scientific Laboratory) (1972).
[5] M. Barbier, *Induced radioactivity* (North-Holland Publ. Co., Amsterdam, 1969).
[6] J. W. Meadows, ANL Report ANL/NDM-18 (1976).
[7] T. K. Khoe and M. Kimura, ANL Report ANL-SSS-74-1 (1974).

[8]) A. S. Arrott and I. M. Thorson, University of British Columbia TRIUMF Project Report TRI-76-XXX (1976).
[9]) J. D. Simpson, IEEE Trans. Nucl. Sci. **NS-20**, no. 2 (1973) 198.
[10]) A. Michaudon, J. Nucl. Energy A/B **17** (1963) 165.
[11]) D. F. R. Mildner and G. C. Stirling, Rutherford Laboratory (UK) Report RL-75-095 (1975).
[12]) M. M. R. Williams, *The slowing down and thermalization of neutrons* (North-Holland, Publ. Co., Amsterdam, 1966).
[13]) K. F. Graham and J. M. Carpenter, Nucl. Sci. Engng. **49** (1972) 418; also K. F. Graham and J. M. Carpenter, Nucl. Instr. and Meth. **85** (1970) 163.
[14]) N. G. Sjøstrand, J. Mednis and T. Nilsson, Ark. Fysik **15** (1959) 471.
[15]) K. Sumita, in *Pulsed neutrons and their utilizations*, Joint Meeting Euratom–Japan Atomic Energy Society, Ispra, Italy (1971) p. 287.
[16]) N. Watanabe, M. Kimura, H. Takahashi and S. Tomiyoshi, ibid., p. 255.
[17]) R. G. Fluharty, F. B. Simpson, G. J. Russel and J. H. Menzel, Nucl. Sci. Engng. **35** (1969) 45.
[18]) Inoue, to be published.
[19]) S. N. Ishmaev, I. P. Sadikov and A. A. Chernyshov, IV Kurchatov Institute (USSR) Report IAE-271 (1973) [Transl. by D. F. R. Mildner as Rutherford Laboratory Report (UK) RL-75-129 (1975)].
[20]) J. M. Carpenter and G. J. Marmer, Informal Argonne National Laboratory Report, ANL-SSS-72-1 (1972).
[21]) S. G. Das, J. M. Carpenter and R. E. Prael, Argonne National Laboratory Report ANL-77-76-123.
[22]) G. J. Russel, P. A. Seeger and R. G. Fluharty, Los Alamos Scientific Laboratory Report LA-6020 (1977).
[23]) D. F. R. Mildner, unpublished report (1976).
[24]) J. B. Vetrano, Nucl. Engng. Design **14** (1970) 390.
[25]) J. M. Carpenter, M. H. Mueller, R. A. Beyerlein, T. G. Worlton, J. D. Jorgensen. T. O. Brun, K. Sköld, C. A. Pelizzari, S. W. Peterson, N. Watanabe, M. Kimura and J. E. Gunning, Proc. *Neutron diffraction* Conf., Petten, The Netherlands.
[26]) K. Sköld, K. Crawford and S. H. Chen, Nucl. Instr. and Meth. **145** (1977) 115.
[27]) Argonne National Laboratory Report 77-76-123.